An Experimental Investigation of Ride Control Algorithms for High-Speed Catamarans

Part 1: Reduction of Ship Motions~~Motion Response to Waves of a High-Speed Catamaran with Feedback Ride Control~~

Javad AlaviMehr[1], Jason Lavroff[1], Michael R. Davis[1], Damien S. Holloway[1], Giles A.Thomas[2]

[1]University of Tasmania
[2]University College London

Abstract

Ride control systems are essential for comfort and operability of high-speed ships, but it remains an open question what is the optimum ride control method. To investigate the motions of a 112 m high-speed catamaran fitted with a ride control system a 2.5 m model was tested in a towing tank. The model active control system comprised two transom stern tabs and a central T-Foil beneath the bow. Six ideal motion control feedback algorithms were used to activate the model scale ride control system and surfaces in a closed loop control system: heave control, local motion control and pitch control, each in a linear and nonlinear version. The responses were compared with the responses with inactive control surfaces and with no control surfaces fitted. The model was tested in head seas at different wave heights and frequencies and the heave and pitch Response Amplitude Operators (RAOs), Response Phase Operators (RPOs) and acceleration response were measured. It was found that the passive ride control system reduced the peak heave and pitch motions only slightly. The heave and pitch motions were more strongly reduced by their respective control feedback. This was most evident with nonlinear pitch control which reduced the maximum pitch RAO by around 50% and the vertical acceleration near the bow by about 40% in 60 mm waves. These reductions were influenced favorably by phase shifts in the model scale system which effectively contributed both stiffness and damping in the control action.

Nomenclature

$C_{L\alpha}$	Control surface lift coefficient derivative ($dC_L/d\alpha$)
Fr	Froude number based on hull waterline length
g	Gravitational acceleration (m/s^2)
H	Model heave at LCG (m, positive up)
*H**	Dimensionless model heave at LCG (heave/wave amplitude)
l	Length of model waterline (m)
LCG	Longitudinal Centre of Gravity

L_{ST} Stern tab lift force (N)

L_{TF} T-Foil lift force (N)

P Model pitch about LCG (radian, positive bow down)

P^* Dimensionless model pitch at LCG (pitch/wave slope)

S_{ST} Stern tab planform area (m^2)

S_{TF} T-Foil planform area (m^2)

$ST0$ Stern tab initial angle of attack (radian, positive producing upward lift)

$TF0$ T-Foil initial angle of attack (radian, positive producing upward lift)

U Model forward speed (m/s)

x_{ST} Distance between centre of pressure of the stern tabs and LCG (m)

x_{TF} Distance between centre of pressure of the T-Foil and LCG (m)

α_{ST} Stern tabs angular deflection (radian, positive producing upward lift)

α_{STd} Control system demand stern tabs angular deflection (radian, positive producing upward lift)

α_{TF} T-Foil angular deflection (radian, positive producing upward lift)

α_{TFd} Control system demand T-Foil angular deflection (radian, positive producing upward lift)

ζ Wave amplitude (m)

λ Wave length (m)

ρ Water density (kg/m^3)

ω_0 Wave frequency in fixed coordinate (radian/s)

ω_e Wave encounter frequency (radian/s)

ω_e^* Dimensionless wave encounter frequency

1. Introduction

Global demand for fast and efficient sea transportation has led to the evolution of large high-speed and lightweight vessels for both commercial and military use [1]. Different types of high-speed craft have been designed to satisfy this requirement, but some factors such as large deck area, relatively large deadweight to displacement ratios, the ability to provide lightweight Ro-Ro vessels (Roll-on/Roll-off vessels capable of carrying wheeled cargo such as cars and trucks) and high hydrostatic and hydrodynamic stability have proven catamarans to be particularly popular [1]. A unique form of high-speed wave-piercing catamarans has been designed and built by INCAT

Tasmania [2], featuring a distinctive short centre bow located on the vessel centreline between the wave-piercer demihulls designed to effectively eliminate deck diving in following seas.

High-speed catamarans, due to their slender twin hull geometry and high operating Froude number [3], frequently experience larger heave and pitch motions and accelerations than those of conventional monohulls operating at lower Froude number. The vessel motions are directly influenced by increases in the operating speed, leading to passenger discomfort and potential structural damage when operating in higher sea states and severe sea conditions [4]. A motion control system is therefore required to reduce these large motions, increase passenger comfort and improve the vessel performance.

INCAT Tasmania [2] uses active motion control systems for its high-speed wave piercing catamarans to reduce vessel motions and dynamic structural loads, improve passenger comfort and increase the range of operability [4, 5]. These active Ride Control Systems (RCS) consist of a retractable T-Foil mounted on the centreline at the aft end of the centre bow and two active trim tabs located at the stern of the vessel demihulls. Figure 1 shows the location of the T-Foil and the trim tabs on a 112 m INCAT Tasmania high-speed wave-piercing catamaran [2] and Figure 2 shows a full scale T-Foil prior to installation [2]. The active T-Foil and trim tabs produce unsteady vertical forces, either downward or upward, to resist heave and pitch motions. Being retractable, removing the T-Foil from operation helps to reduce resistance in calm water. The trim tabs installed at the stern of the vessel demihulls, hereafter called stern tabs, generate a lift force at the transom to retain the desired vessel dynamic trim and reduce pitch and heave motion in combination with the T-Foil. The stern tabs can also resist the vessel roll motion when they are operated differentially.

There have been some prior studies of ride control systems relevant to this type of fast ships. The problem has been tackled both experimentally and numerically. In 1995, the development of a ride control system for fast ferries [6] and the role of simulation in this development [7] were investigated by Haywood et al. In 2015, Haywood et al. reviewed the different ride control devices including fins, trim tabs, interceptors, retractable T-Foils and lifting foils by studying technical aspects, costs, ease of installation, operational and maintenance requirements and material [8]. In 2000, Esteban et al. investigated the vertical acceleration reduction of a monohull fast ferry with the control of flaps and T-Foil by control-oriented modelling [9]. This work was extended in 2001 by Esteban et al. to attenuate the ship's vertical motions by a simulation tool using MATLAB and SIMULINK [10]. This numerical investigation was extended in 2001 by experimental study conducted by Giron-Sierra et al. [11]; however, these experiments only studied the reduction of the acceleration and MSI. In

2002, Giron-Sierra et al. studied the control of the actuators for vertical motion damping [12] and concluded that not only did the MSI need to be minimized, but other objectives such as reduced control effort, vibrations and cavitation should be considered [12]. In 2002, Esteban et al. investigated the multiobjective optimization of control by designing a Genetic Algorithm method [13]. In 2003, a complete control-oriented model was used by Giron-Sierra et al. [14] to study PID control of fast ferries and it was shown that moving controlled actuators can have an important stabilisation effect. In 2004, Esteban et al. developed the control-oriented model of the vertical motions of the fast ferry by a methodology based on MATLAB tools using experiments and CAD-based programs [15].

In 2002, reduction of the vertical motion of a round-bilge boat in waves by design of controllable transom flaps was investigated by Wu-Qiang et al. [16] and this was evaluated by some model tests. However, an oscillating flap was used instead of a controllable flap for evaluation of the effects of flaps on pitch reduction of the model [16]. These model experiments have shown that using an oscillating flap would reduce pitch motion, if a suitable phase could be established between flap exciting forces and wave disturbances [16]. In 2004, Sclavounos et al. studied the seakeeping performance of a foil-assisted high-speed monohull vessel using a state-of-the-art three-dimensional Rankine panel method where it was found that the most efficient location for the hydrofoil is at the ship bow leading to a 50% reduction of the root mean square values of the heave and pitch motions in a Joint North Sea Wave Project (JONSWAP) spectrum [17]. In 2011, seakeeping simulations for a high speed wave piercing catamaran with an active ride control system was carried out by Hughes et al. using the Large Amplitude Motion Program (LAMP), a time domain potential flow panel code that solves the 3-D wave-body hydrodynamics and rigid-body dynamics problems [18]. Hughes et al. concluded that the LAMP predictions show a significant benefit from actively controlled trim tabs and T-Foils for reducing both pitch and roll motions [18]. In 2011, Rijikens et al. developed a computational tool for the design and optimization of the ride control systems for high speed planing monohulls where their simulations demonstrated improvement in motion behaviour of a fast planing vessel with a ride control system sailing in head waves [19]. Rijikens et al. also investigated the hydrodynamic performance of a new transom-interceptor configuration to control the motion behaviour of a fast ship in waves in 2013 where it was found that the new transom interceptor configuration leads to reduction of accelerations which contributes to a more favourable sea keeping performance of the ship [20].

Although the above investigations into ship motion control systems on fast ships have been undertaken by numerical computations, model experiment and full-scale sea trials, there is still limited knowledge of the

mechanisms of the whole motion control system. In particular, the best control algorithm for linking detected ship motions to control surface activity has yet to be determined. In order to understand and optimise the motion control system further investigation is therefore required to accurately determine the effect of the control algorithm on the ship motions. The overall objective of the current research is to evaluate the effect of the ride control algorithm on motions in waves under more controlled conditions than is possible at full scale. The motions data at model scale, in conjunction with full scale sea trials data and numerical computations will ultimately assist in the optimisation of motion control system algorithms to improve ship motions, passenger comfort and reduce structural loads.

2. Model set-up and instrumentation

An existing 1/44.8 scale 2.5 m catamaran model of the 112 m INCAT Tasmania wave-piercing catamaran was used for the tank tests. The development of the catamaran model has been previously described by Lavroff et al. [21-24]. Although active ride control systems have been installed on all full scale 112m INCAT Tasmania wave-piercer catamarans, the 2.5m hydroelastic segmented model did not originally include an active ride control system in the previous model tests [21-24]; stern tabs were statically mounted to correct bow up trim at speed and no T-Foil was fitted to the model. Therefore a model scale T-Foil has been developed [25, 26] to fit to the model and the fixed tabs were replaced with moveable tabs. Figures 3 and 4 show the electrically activated model scale T-Foil and stern tabs respectively, while Table 1 shows their specifications. It is to be noted that the model scale T-Foil was pivoted within the model foil itself at the base of a rigid mounting strut whereas the full scale T-Foil and strut (Figure 2) were rigidly connected and were both mounted on a pivot within the hull. The model configuration was chosen so that the model pivot was located slightly ahead of the model T-Foil centre of pressure thereby minimising the power required to move the model foil. Given the limited power of the model servo-motor this arrangement maximised the response rate of the model system. Three servo-motors were used to independently activate the T-Foil and stern tabs, while three potentiometers measured their angular positions. Figures 5 and 6 show the T-Foil and its electrical actuator installed on the aft section of the centre bow. Figure 7 shows the stern tabs installed at the aft end of the model.

In order to effectively activate the control surfaces according to vessel motions it was important to conduct dynamic tests on the T-Foil and stern tabs to investigate their performance prior to installation for testing on the 2.5 m catamaran model. A previous investigation has been conducted on the lift and drag characteristics as well as frequency response of the model scale, low Reynolds number T-Foil by both static and dynamic tests [25]. The

model scale T-Foil operates at a Reynolds number of approximately 10^5, has an aspect ratio of 3.6 and a planform which is strongly tapered from the inboard to the outboard end. It was concluded from the previous study [25] that the unsteady performance of the low Reynolds number model scale T-Foil with a relatively low aspect ratio was adequate for application to scale model towing tank tests. Studies of the lifting performance of the model scale stern tabs have also been undertaken at the University of Tasmania [27, 28].

A previous study [26] investigated the step and frequency responses of the 112 m INCAT catamaran to the ride control system by calm water open-loop testing of the 2.5 m catamaran model ride control system. These open loop responses provided essential data for setting up the control system for the current study of the closed-loop active control system. A specific outcome of the previous open loop study was to find an appropriate combination of control movements to excite the model only in heave or only in pitch [26]. This formed the basis of setting the gains of the ride control system for the current investigation to implement different motion control methods for pitch control, local motion control and heave control. By local control we mean that each control surface operates effectively independently to control vertical motion at the location of that control surface, a method implemented in some control systems essentially mimicking the action of a vehicle suspension system by introducing local vertical motion stiffness and damping.

Model testing for the present work was conducted at the Australian Maritime College (AMC) towing tank in Launceston, Tasmania, with a model displacement of 28.3 kg simulating a full scale displacement of 2545 tonnes. The towing tank is 100 m long, 3 m wide and 1.4 m deep. The model was attached to the moving carriage using two tow posts mounted forward and aft of the model longitudinal centre of gravity (LCG). Figure 8 shows the model attached to the moving carriage.

A National Instruments (NI) 9174-USB compact DAQ (cDAQ) chassis was used to record the dynamic tank tests and operate the feedback control system with two NI modules, a NI 9263 Analogue Output (AO) and a NI 9201 Analogue Input (AI) module. Control surface deflections were demanded through the AO module and the AI module acquired the potentiometer voltage to measure the actual instantaneous deflection of the control surfaces. Three additional voltages indicating carriage speed, forward tow post motion (a Linear Variable Differential Transformer, LVDT) and aft tow post motion (LVDT), were logged using the NI 9201 Analogue Input (AI) module. The servo-motors and the potentiometers were calibrated to determine the relationship between demand voltage for the servo-motor and relative deflection of the control surface, and the relationship between the output voltage from the potentiometer and relative deflection of the control surface. During calibration the deflections of

the control surfaces were measured using a digital inclinometer with a resolution of 0.05º. The inclinometer was aligned with the T-Foil chord line and the stern tabs lower surface, with 0º corresponding to these being parallel to the model nominal calm waterline.

Although the RCS DAQ system was able to log all the required data, a separate towing carriage data acquisition and signal conditioning system was used simultaneously to cross check the data acquired by the RCS DAQ system. The outputs of the two LVDTs mounted on the tow posts were recorded and their vertical movements used to calculate model heave and pitch. Two video cameras were set up to record all the runs from bow and stern views. A LabVIEW program was written to activate the ride control surfaces in a closed-loop system using the model motion LVDT inputs, the chosen ride control feedback algorithm and the relative control gains, as described in the following section.

3. Ride control algorithms

The towing tank model was tested with different ride control conditions including without RCS (i.e. no T-Foil and locked stern tabs), passive RCS (i.e. with locked T-Foil and stern tabs) and active RCS. The active RCS modes consisted of heave control, local motion control and pitch control, while linear and nonlinear gains were applied for each control mode. The linear gains were selected so that the control motions remained within their maximum range of physical movement, the nonlinear gains were set at large values so that the control surfaces moved at maximum slew rate between their extreme positions, thus generating maximum control force at all times. The general equations for demanded deflection for each control surface for all algorithms based on global motions are

$$\alpha_{TFd} = TF0 + aH + b\dot{H} + c\ddot{H} + dP + e\dot{P} + f\ddot{P} \quad (1)$$

$$\alpha_{STd} = ST0 + gH + h\dot{H} + i\ddot{H} + jP + k\dot{P} + l\ddot{P}, \quad (2)$$

where α_{TFd} and α_{STd} are the demanded T-Foil and the stern tab deflections respectively, *TF0* and *ST0* are the T-Foil and the stern tab initial angles respectively, *H* and *P* are the instantaneous heave and pitch, and the parameters *a* to *l* are the control gains. Over dots represent differentiation with respect to time.

At this point we need to note that the small model scale control system has physical limitations due to its size. In particular it is known to have phase lags between demands and control motions [25]. In general, commercial full scale ride control systems are operated as motion damping systems with the broad objective of reducing peaks in RAOs under circumstances of relatively small control forces (e.g. several hundred tonnes weight) in proportion to ship weight (e.g. several thousand tonnes). Under such conditions it appears that the control system is not capable of significantly modifying system stiffness and so control action is primarily directed at motion control by

damping. However, some commercial systems do incorporate a small stiffness effect in the feedback, particularly for pitch control. In the present model scale investigation we have taken the approach of formally implementing damping feedback in the control system but we must recognise that phase lags in the model system give rise to an effective combination of damping and stiffness in the control action.

Equations 1 and 2 can be simplified by considering only damping modes of feedback demand to the control surface actuators and zero magnitude of initial control surfaces deflection, giving

$$\alpha_{TFd} = b\dot{H} + e\dot{P} \qquad (3)$$

$$\alpha_{STd} = h\dot{H} + k\dot{P}. \qquad (4)$$

Here α_{TFd} and α_{STd} represent demanded pitch deflections of the T-Foil and stern tabs, the actual deflections being somewhat phase lagged from these demands [25].

3.1. Pitch control

Equations 3 and 4 can be further simplified to give equations for the demanded control deflections for the pitch control as

$$\alpha_{TFd} = e\dot{P} \qquad (5)$$

$$\alpha_{STd} = k\dot{P}. \qquad (6)$$

Once again, these are the demanded control deflections and the actual control deflections will be somewhat phase lagged to the demanded deflections. The gains *k* and *e* must have a defined ratio to ensure that no net heave force is generated but only a pitch control moment. To calculate the parameter *e* for the linear deflection of the T-Foil, the maximum T-Foil deflection should be considered in relation to an estimated maximum pitch velocity. Thus, noting that a positive T-Foil force produces a negative pitching moment,

$$e = -\frac{(\alpha_{TFd})_{max}}{\dot{P}_{max}}. \qquad (7)$$

Equation 7 can be solved with the following inputs:

- Maximum pitch rate, $\dot{P}_{max} = P_{max} \times \omega_e$
- Wave encounter angular frequency, $\omega_e = \omega_e^* \sqrt{\frac{g}{l}}$
- Maximum pitch, $P_{max} = (\text{Maximum wave slope}) \times (\text{Maximum pitch RAO})$ where

  Maximum wave slope $= \frac{2\pi\zeta}{\lambda}$, ζ= wave amplitude and $\lambda = \frac{2\pi g}{\omega_0^2}$ is the wavelength.
- The wave angular frequency in fixed coordinates,

$$\omega_0 = \omega_0^* \sqrt{\frac{g}{l}} = \frac{-1 + \sqrt{1 + (4\omega_e^* Fr)}}{2Fr} \sqrt{\frac{g}{l}}$$

- The Froude number, $Fr = \frac{U}{\sqrt{gl}}$ where U = model forward speed, g = gravitational acceleration and l = model length.

In order to activate the ride control system in the pitch control mode, the total net force of control surfaces in the heave direction should be zero. It was assumed that the drag component of each control surface is negligible in the heave direction. It is also assumed that the control surfaces are sufficiently close to the hull that the local flow is parallel to the hull and therefore the control surfaces respond only to their deflections relative to the hull, i.e. there is no additional effective angle of attack resulting from the global pitching of the model. Thus the lift forces are

$$L_{TF} = \frac{1}{2}\rho U^2 S_{TF} \alpha_{TF} (C_{L\alpha})_{TF} \qquad (8)$$

$$L_{ST} = \frac{1}{2}\rho U^2 S_{ST} \alpha_{ST} (C_{L\alpha})_{ST}, \qquad (9)$$

where $\alpha_{TF}$and α_{ST} are actual surface deflections. For zero heave force we require $L_{TF} + 2L_{ST} = 0$ (noting that there are two tabs), therefore

$$\frac{\alpha_{ST}}{\alpha_{TF}} = \frac{-S_{TF}(C_{L\alpha})_{TF}}{2S_{ST}(C_{L\alpha})_{ST}}. \qquad (10)$$

Combining Equation 10 with Equations 5 and 6, the control parameter k for the linear deflection of stern tabs is evaluated as

$$k = -e\frac{S_{TF}(C_{L\alpha})_{TF}}{2S_{ST}(C_{L\alpha})_{ST}}, \qquad (11)$$

where the control surfaces lift coefficient derivative ($C_{L\alpha}$) were determined based on the results from previous studies on the T-Foil [25] and stern tabs [27]. It should be noted that during control operations the T-Foil reaches the limit of its range before the stern tabs when the actions are balanced to give zero heave. Therefore the parameter e is determined by equation 7 in terms of the maximum T-Foil deflection and the parameter k is determined by equation 11 in terms of e. Thus, whilst the T-Foil can operate over its full range of action, the stern tabs operate at less than their full range of action in this control mode.

3.2. Heave control

In order to evaluate the control gains for the heave control Equations 3 and 4 are reduced to equations for the demanded control deflections:

$\alpha_{TFd} = b\dot{H}$ (12)

$\alpha_{STd} = h\dot{H}.$ (13)

The parameter b is evaluated by considering the maximum deflection of the T-Foil and the maximum heave velocity,

$b = -\frac{(\alpha_{TFd})_{max}}{\dot{H}_{max}},$ (14)

where the maximum heave velocity is

$\dot{H}_{max} = H_{max} \times \omega_e$

and maximum heave is

$H_{max} =$ (Maximum wave amplitude) × (Maximum heave RAO).

For the heave control mode the total pitch moment about the LCG induced by the control surfaces must be zero, thus $L_{TF}x_{TF} - 2L_{ST}x_{ST} = 0$, giving

$h = b\frac{x_{TF}S_{TF}(C_{L\alpha})_{TF}}{x_{ST}2S_{ST}(C_{L\alpha})_{ST}},$ (15)

where x_{TF} and x_{ST} are the distances between the LCG and the centre of pressure of the T-Foil and the stern tabs respectively. Once again the T-Foil reaches the limit of its range before the stern tabs when the actions are balanced to give zero pitch. Therefore the parameter b is determined by equation 14 in terms of the maximum T-Foil deflection and the parameter h is determined by equation 15 in terms of b.

3.3. Local control

In order to control the local control surface motions, the control surfaces act independently and have input demands to oppose the local vertical velocities. The vertical velocity of the model at the longitudinal location of each control surface are $\dot{H} - x_{TF}\dot{P}$ and $\dot{H} + x_{ST}\dot{P}$ for the T-Foil and stern tab respectively. Thus from Equations 3 and 4 we require control surface demands $\alpha_{TFd} = b(\dot{H} - x_{TF}\dot{P})$ and $\alpha_{STd} = h(\dot{H} + x_{ST}\dot{P})$, where

$b = -\frac{(\alpha_{TFd})_{max}}{\dot{H}_{max}}$ (16)

$h = -\frac{(\alpha_{STd})_{max}}{\dot{H}_{max}}.$ (17)

Written in the form of Equations 3 and 4 we thus specify

$$e = -b \times x_{TF} \quad (18)$$

$$k = h \times x_{ST}. \quad (19)$$

3.4. Nonlinear control algorithms

It is recognised that the control surfaces are not large enough to cancel motions altogether in large waves. Therefore a nonlinear version of each algorithm is proposed, in which the control surfaces are moved to their maximum angular offsets as quickly as the mechanisms will allow, thus giving demand control surface deflections

$$\alpha_{TFd} = \pm b\dot{H}_{max} \pm e\dot{P}_{max} \quad (20) \text{ and}$$

$$\alpha_{STd} = \pm h\dot{H}_{max} \pm k\dot{P}_{max}. \quad (21)$$

The constants b, e, h and k are determined as described above for the respective operation mode, and the sign in each case is chosen so that the lift force or moment opposes the relevant velocity term (heave, pitch or local). While this does not change the maximum control forces at maximum control defection at the extreme point of the motion vertical velocity, it will maintain the forces at maximum values opposing the velocities for a longer duration within the motion half cycles and so increase the impulse of those forces by a factor of approximately $\frac{\pi}{2}$ (an additional 57%) assuming the motions to be close to sinusoidal and the control mechanisms to be instantaneously responsive. This represents a significant potential increase of motion control performance.

4. Motion tests and analysis

Towing tank testing in head seas was undertaken in regular waves at a model speed of 2.89 m/s, simulating a full scale speed of 37 knots. The model was tested at two wave heights, 60 mm and 90 mm, simulating full scale wave heights of 2.69 m and 4.03 m respectively. Wave frequencies ranging from 0.350 Hz to 0.900 Hz were generated by the towing tank wave maker for each test condition. Table 2 summarises the model test conditions.

As can be seen in Table 2, the model tests in 60 mm waves were conducted with different control conditions including without RCS, passive RCS, linear heave control, nonlinear heave control, linear local control, nonlinear local control, linear pitch control and nonlinear pitch control. In contrast, the model tests in 90 mm waves were only carried out with control conditions of passive RCS, linear heave control, linear local control, linear pitch control and nonlinear pitch control. The results obtained in 60 mm waves demonstrated that the nonlinear ride control system was not more effective than the linear system in heave and local control modes.

Figure 9 shows a typical sample time record at a model speed of 2.89 m/s (Fr = 0.608), a wave height of 90 mm and dimensionless wave encounter frequency ω_e^* = 3.182 for the passive RCS mode and pitch control mode. It is to be noted that the wave profile at the LCG and the heave motion are positive up, the pitch motion is positive bow down and the control surfaces deflection are positive counter-clockwise viewed from the starboard side, producing upward lift. In order to evaluate the amplitude and phase of the signals, a range of the time record was analysed, starting when regular periodic motions had been reached and including at least five cycles, and an average of all these cycles is presented. The amplitude and phase analysis was carried out by finding the peak and trough of each cycle. As can be seen from Figure 9, the pitch control mode significantly reduced the pitch motion, clearly demonstrating the significant effect of motion control on the response of the model in this mode.

5. Ride control system motions response

5.1. Uncertainty analysis

In order to establish the accuracy of the results an uncertainty analysis was performed based on the standard deviation of the results. For each run the time record included from 5 to 19 useable cycles after transients had dissipated and before either the run terminated or reflections or other forms of contamination became significant. The variation between the cycles in each run was analysed in order to quantify the accuracy of the results. The standard deviation analysis of the results shows an average of ±2.5% variation for the wave elevation, ±2.0% variation for the heave motion and ±2.2% variation for the pitch motion. Figures 10 and 11 illustrate these uncertainty results for some typical cases at a wave height of 60 mm, showing the error bars on the dimensionless pitch and heave respectively. Three of the ride control conditions including without RCS, pitch control and nonlinear pitch control were selected for demonstrating the error bars on the dimensionless pitch shown in Figure 10, while three ride control conditions: without RCS, heave control and nonlinear heave control, were chosen to show the error bars on the dimensionless heave demonstrated in Figure 11. These curves illustrate the substantial changes brought about by the most successful ride control algorithm, but as can be seen from Figures 10 and 11, the uncertainty in the results within each case is insignificant compared to the overall effect of the ride control system. Thus the experimental uncertainty has no impact on the key conclusions of this research, and in view of the quantity of data subsequent results will be presented without error bars.

It should be noted that all of the experimental set-up was calibrated prior to model tests and zeros were taken before each run. Items such as LVDTs and wave probes were calibrated daily. Therefore in addition to the uncertainty analysis, the bias error of the experimental set-up was estimated by comparing the daily calibration

factor to quantify any possible drift. This showed an average fluctuation of about ±1.5% which clearly demonstrates the insignificant magnitude of the systematic errors. There are other effects that may be difficult to quantify precisely, for instance carriage aerodynamic effects as reported by Yang [29] in the same towing tank as used in the present experiments. Yang demonstrated that there was flow of air between the top of the carriage and the water surface that caused a pressure wave in the vicinity of and travelling with the test model, and a corresponding reduction in the local calm water surface height. However, this phenomenon will affect different tests in the same way, so will not change the ranking of results, nor the conclusions.

5.2. Response Amplitude Operators (RAOs)

The heave and pitch motions were measured using the LVDT data obtained from the towing tank data acquisition system and from this the Response Amplitude Operators (RAOs) were evaluated. Figures 12 and 13 show the pitch RAO at wave heights of 60 mm and 90 mm respectively and Figures 14 and 15 show the heave RAO at wave heights of 60 mm and 90 mm respectively. In addition to the different control conditions, the results from a previous study with no ride control conducted on the same model by Lavroff [23] are presented in these figures to compare with the current results.

Comparing the results of the model tests without RCS and with a passive RCS it can be seen that the deployment of the T-Foil to a fixed position and acting as a passive control surface reduces the peak heave and pitch motions. As expected, heave and pitch were more strongly reduced by their respective control algorithms. This was more evident in the pitch control mode, where the pitch RAO is substantially reduced. Operation in local control mode led to similar results to those from operation in the heave control mode.

Figures 12 and 13 demonstrate that compared to the passive RCS mode, the local control algorithms increased the pitch motion at dimensionless wave encounter frequencies (ω_e^*) up to 4. A similar trend can be seen for the heave control mode, however it reduced the pitch motion at very low wave frequencies. As can be seen from Figure 12, the nonlinear action of the ride control system in the heave control mode increased the pitch motion and a clear benefit of nonlinearity could not be identified in the local control, although it shows some pitch motion reduction at very low wave frequencies. The most notable aspect of the data presented in Figures 12 and 13 is the significant effect of the nonlinear pitch control algorithm on the reduction of model pitch motion, where it reduced the peak pitch motion by about 50%.

As expected, Figures 14 and 15 show that heave motion was reduced by the heave control algorithm and was more strongly reduced in the nonlinear heave control mode. A similar outcome was obtained by the linear and nonlinear

local motion control algorithms. Although the pitch control mode had a positive effect for $\omega_e^* > 3.5$, this control mode increased the heave motion at low frequencies.

In general the pitch control and heave control modes strongly reduced the pitch and heave motions respectively for all cases investigated. The nonlinear control modes demonstrated the most significant effect on reducing the motions response of the model, in particular when compared to the non RCS results of Lavroff [23] with a reduction of up to 50% in pitch motion.

5.3. Response Phase Operators (RPOs)

In addition to the RAOs, the Response Phase Operator (RPO) was studied at different wave heights and frequencies, because of the importance of phase lag between the wave profile and model motions. The pitch RPO is the phase lag of the model pitch motion relative to the wave profile measured at the model LCG. Similarly the heave RPO is the phase lag of the heave motion relative to the wave profile at the model LCG. In order to measure the phase lag of the model motions relative to the wave profile, a time record of recorded data that included at least five cycles of each signal was analysed. The peaks and troughs of the signals were found and an average of all cycles was evaluated.

Figures 16 and 17 show the pitch RPO at wave heights of 60 mm and 90 mm respectively, while Figures 18 and 19 show the heave RPO at wave heights of 60 mm and 90 mm respectively. As can be seen from Figures 16 and 17, the pitch RPO tends to 90° at very low wave frequencies, as expected since the pitch follows the wave slope. These figures also show that there is a progressive increase of phase lag of pitch relative to the encountered wave with increasing wave frequency, indicating an increasing lag as inertia becomes more significant at higher frequency. The increase of phase lag from zero to high frequency however remains below 180° in all cases, reaching about 120° of lag increase in the smaller waves and about 70° of lag increase in the larger waves. Broadly similar increases of 120° and 70° in phase lag with frequency in smaller and larger waves respectively are seen in the heave responses shown in Figures 18 and 19. However, the heave RPOs commence at 0° at low wave frequencies. Overall, we see that the pitch motion lags the heave motion by approximately 90° over the full range of frequencies tested which extends well beyond the frequency of maximum motions (at about $\omega_e^* \sim 4$) into the frequency range of quite small motions ($\omega_e^* > 6$ approximately).

Since the controls are mechanical systems with inertia and a limited slew rate of about 300 degree/s it is to be expected that their response will lag demand inputs. Although the ride control algorithms were designed on the

basis of the control gains as explained in section 3, any phase lag between the control surfaces deflection and model motions will appear as an increased effective stiffness of the control system.

Figures 20 and 21 show the phase lag of the T-Foil relative to pitch at wave heights of 60 mm and 90 mm respectively. It should be noted that all phase data are presented in the range from 0° to 360°, therefore +360° was added to the negative results in order to present them in the positive zone of the phase lags. As can be seen from Figures 20 and 21, in pitch control mode the phase lag between detected motion and T-Foil movement lies between 270° and 360°. This corresponds to the control force comprising both damping and stiffness components. With heave or local motion control the phase lies between 0° and 90°, this also corresponding to the T-Foil force comprising both damping and stiffness components. When the system operates with higher nonlinear gains the limited slew rate of the model mechanism increases the phase lag in both modes of control. Similar effects are evident in the phase lag of the stern tabs shown in Figures 22 and 23, where in pitch control mode the phase lag lies between 90° and 180° approximately; this again corresponds to the control force being a mix of damping and stiffness components.

5.4. Acceleration response

Although the ride control system has demonstrated significant effect in reducing the motion response of the catamaran model, the effect of the ride control system on the passenger comfort depends primarily on the vertical accelerations measured on the catamaran model. Furthermore, depending on the magnitude and phase of heave and pitch motions, the accelerations can be quite different at different locations on the hull. The vertical motion acceleration of the catamaran model was therefore investigated at three different longitudinal locations consisting of LCG, the longitudinal location of the T-Foil and the longitudinal location of the stern tabs. The longitudinal location of the LCG and the T-Foil are 37% and 80% of LOA from the stern respectively, and the location of the T-Foil and the stern tabs represent approximate forward and aft most locations that passengers might be expected to occupy. Given that motions are close to sinusoidal, dimensionless heave accelerations were simply calculated by

$$\ddot{H}_x^* = H_x^* \times \omega_e^{*2} = \ddot{H}_x \frac{l}{g\zeta} \ , \qquad (22)$$

where the subscript $_x$ refers to the location at which the motion was analysed.

The heave motion at the longitudinal location of the T-Foil and stern tabs were calculated respectively by

$$H_{TF}(t) = H(t) - x_{TF} \times P(t) \qquad (23)$$

$$H_{ST}(t) = H(t) + x_{ST} \times P(t) \ . \qquad (24)$$

Figures 24 and 25 show the dimensionless heave acceleration at the LCG at wave heights of 60 mm and 90 mm respectively. As can be seen from Figures 24 and 25, the ride control system reduced the heave acceleration at the LCG even in the passive mode. As would be expected, there is a significantly larger reduction of accelerations in smaller waves as the control system gains were set higher in the smaller waves so that the controls were acting with close to maximum range of movement at both wave heights. Figures 26 and 27 show the dimensionless vertical acceleration at the longitudinal location of the T-Foil at wave heights of 60 mm and 90 mm respectively. The accelerations at this forward location are much greater than at the LCG by a factor of about 2.5 showing that these forward on board locations are far less suitable for passenger accommodation. However, we see that the RCS in the pitch control mode has achieved approximately 40% reduction of these forward accelerations in the smaller waves. The dimensionless vertical acceleration at the location of the stern tabs at wave heights of 60 mm and 90 mm are shown in Figures 28 and 29 respectively. Here again the pitch control mode achieves a 40% reduction of vertical accelerations in the smaller waves. Overall the accelerations were greatest at the forward T-Foil location and smallest at the LCG, the forward accelerations being approximately 2.5 times those at the LCG and the stern acceleration being about 1.9 times the LCG acceleration. The pitch control algorithm, especially in the nonlinear mode, demonstrated the strongest influence in reducing the vertical accelerations, which is the most important factor to improve passenger comfort.

The results presented here can be used to determine the effect of the RCS on passenger motion sickness incidence (MSI). However, that determination depends very much on the spectrum of the encountered waves and so it is not possible to give a single answer as to the benefit of the RCS on MSI values. The MSI equation presented by O'Hanlon et al. [30] demonstrates that there are many factors affecting the MSI such as wave encounter frequency, acceleration and some parameter with values determined empirically. However in the range where MSI increases most rapidly with acceleration it is found that a 40% reduction of acceleration would approximately reduce the MSI by up to 50% [30].

5.5. Control surfaces response amplitude

During these experimental tests of the model with active RCS it was necessary to set pre-determined and fixed control system gains for each mode of control action. These gains were determined on the basis of the estimated maximum motion velocities relevant to each control mode as have been outlined in section 3. Therefore it is of interest to determine the actual variation of control movement with encounter frequency, as in conditions of

smaller motion the controls during these tests would not be acting over their maximum range of movement. This is an inevitable consequence of setting fixed control system gains.

Figures 30 and 31 show the range of T-Foil deflection for different ride control modes with wave heights of 60 mm and 90 mm respectively. The stern tabs deflection range with wave heights of 60 mm and 90 mm are presented in Figures 32 and 33 respectively. As expected the maximum T-Foil deflection of ±10° (range of 20°) and the maximum stern tabs deflection range of 18° (from 0 to +18°) were observed at all wave frequencies for all the nonlinear modes.

Figures 30 and 31 show a T-Foil range of 10° at $\omega_e^* = 2$ for the pitch control mode, which rises to the maximum range of 20° as ω_e^* increases to 3.5 near the peak model motions. The T-Foil range remains steady at ω_e^* in the range 3.5–5 and then decreases to 8° at ω_e^*=7.5. A similar trend can be seen for the heave and local control modes, however the T-Foil range reduces more strongly at ω_e^* above 4 for these two control modes. It can be seen from Figure 32 that the local control algorithm causes the stern tabs to reach their maximum range of deflection at lower wave frequencies. The sterns tab deflections for the pitch control mode has the maximum range of 18° at $\omega_e^* = 4.5$ while the heave control mode does not excite the stern tabs sufficiently to deflect to their maximum range. Figure 33 shows a similar trend for all the ride control algorithms in 90 mm waves, although the maximum range of stern tab deflections is not observed for the heave and local control.

These tests with linear control modes show that the control surface deflections rise from small values at low wave frequencies, where the vertical motion velocities are small, to close to the maximum range of movement at the wave frequencies of peak motions and then reduce to small values at high encounter frequency. However it should be borne in mind that where the control gains are balanced so as to give only heave or only pitch control response, the ratios of control gains must take on specific values as explained in section 3. Therefore it is not possible that both T-Foil and stern tabs in the heave and pitch control modes can be set to operate over their maximum range of movement. For this reason we see that the stern tabs are frequently not operating over their maximum range at the frequency of maximum motion. However, it is evident that the estimations of appropriate control gain for each control mode have generally resulted in operating one of the control surfaces, usually the T-Foil, over its maximum range at the frequency of maximum motion. It can be noted from these results that there would be potential for further improving the performance of the RCS if the control gains were set by an automatic adaptive system so that whatever the wave conditions the RCS would be operating with maximum control movements.

6. Conclusions

In order to investigate the influence of different ride control methods on the motions of a 112 m INCAT high-speed wave-piercing catamaran a 2.5 m model was tested in the Australian Maritime College (AMC) towing tank with six different active ride control methods, a passive system and no system in head seas at different wave heights and frequencies. The Response Amplitude Operators (RAOs), Response Phase Operators (RPOs) and acceleration response of the model were determined using the heave and pitch data. The range of control surface deflections as well as the phase lag between the control surface deflections and the model motions were evaluated in order to investigate the performance of the model ride control system and the effectiveness of the different control methods. The active ride control systems were operated with heave control, local control and pitch control, each with linear and nonlinear operation.

It was found that the deployment of the T-Foil to a fixed position and acting as a passive control surface provides a modest reduction of the peak heave and pitch motions. The heave and pitch motions were much more strongly reduced with active ride controls. This was most evident with the pitch control modes where the nonlinear control action substantially reduced the pitch RAO by about 50% in 60 mm waves at model scale. The pitch motion was larger when the ride control system was operated in the nonlinear heave control mode, however the nonlinearity did not have significant effect on the pitch motions when applied in the local control mode.

The local vertical acceleration of the model at different longitudinal locations was significantly reduced by the ride control system. As was expected, this reduction was most obvious with pitch control, especially in the nonlinear mode, where it reduced the vertical acceleration near the bow by around 40% in 60 mm waves at model scale. The acceleration response of the catamaran model to the ride control system showed the potential for substantial improvement of passenger comfort and potentially reducing the structural loads, particularly with non-linear pitch control where motion sickness incidence could be reduced by as much as 50% depending on encountered wave conditions.

The model RCS introduced significant phase lags between detected motions that generate the demand control deflections and the actual control deflections. The consequence of this was that the control action comprised a mixture of damping and stiffness feedback. However, in the case of pitch feedback control the presence of a significant stiffness component in the actual control actions was found to give substantial reductions in RAO in the lower range of encounter frequency.

The nonlinear control modes produced the maximum T-Foil and stern tab deflection ranges at all wave encounter frequencies. The linear control modes showed maximum range of movement only at the frequency of maximum

motion due to operation with fixed control gains. These results thus show that there is significant potential for the application of adaptive gain control depending on the prevailing sea conditions. Also the nonlinear operation of the control surfaces gives generally the best overall improvement of RAO where the pitch control mode is most effective for improvement of passenger comfort.

In conclusion, the motions response results obtained here demonstrate the potential for significant benefit being obtained by using improved ride control algorithms. There is thus good potential for improving passenger comfort and reducing the incidence of motion sickness, an important consideration in particular for vessels operating in more exposed sea routes.

7. Acknowledgements

This project is supported by Australian Research Council *Linkage* grant No. LP-0883540. The support of INCAT Tasmania Pty. Ltd., Revolution Design Pty. Ltd., the University of Tasmania, and the Australian Maritime College is gratefully acknowledged.

8. References

[1] G. Thomas, S. Winkler, M. Davis, D. Holloway, S. Matsubara, J. Lavroff, *et al.*, "Slam events of high-speed catamarans in irregular waves," *Journal of Marine Science and Technology,* vol. 16, pp. 8-21, Mar 2011.

[2] http://www.incat.com.au/#. (2014).

[3] M. R. Davis and D. S. Holloway, "Motion and passenger discomfort on high speed catamarans in oblique seas," *International shipbuilding progress,* vol. 50, pp. 333-370, 2003.

[4] G. Jacobi, G. Thomas, M. Davis, D. Holloway, G. Davidson, and T. Roberts, "Full-scale motions of a large high-speed catamaran: The influence of wave environment, speed and ride control system," *International Journal of Maritime Engineering,* vol. 154, pp. A143-A155, 2012.

[5] G. Jacobi, G. Thomas, M. R. Davis, and G. Davidson, "An insight into the slamming behaviour of large high-speed catamarans through full-scale measurements," *Journal of Marine Science and Technology,* vol. 19, pp. 15-32, Mar 2014.

[6] A. Haywood, A. Duncan, K. Klaka, and J. Bennett, "The development of a ride control system for fast ferries," *Control Engineering Practice,* vol. 3, pp. 695-702, 1995.

[7] A. Haywood, A. Duncan, K. Klaka, and J. Bennett, "The use of simulation in the development of a ride control system for fast ferries," in *Proc. Conf. Maneuvering and Control of Marine Craft*, 1994, pp. 261-269.

[8] A. Haywood, B. Schaub, and C. Pappas, "Recent developments in ride control," *Proceedings of FAST 2015, 13th International Conference on Fast Sea Transportation,* 2015.

[9] S. Esteban, J. M. Giron-Sierra, J. de la Cruz, B. De Andres, J. Díaz, and J. Aranda, "Fast ferry vertical accelerations reduction with active flaps and t-foil," in *5th IFAC Conference on Manoeuvring and Control of Marine Crafts MCMC2000. Aalborg*, 2000.

[10] S. Esteban, B. De Andres, J. Giron-Sierra, O. Polo, and E. Moyano, "A simulation tool for a fast ferry control design," in *Proc. IFAC Intl. Conf. Control Applications in Marine Systems*, 2001.

[11] J. Giron-Sierra, S. Esteban, B. De Andres, J. Diaz, and J. Riola, "Experimental study of controlled flaps and T-foil for comfort improvement of a fast ferry," in *Proc. IFAC Intl. Conf. Control Applications in Marine Systems*, 2001.

[12] J. M. Giron-Sierra, R. Katebi, J. M. de la Cruz, and S. Esteban, "The control of specific actuators for fast ferry vertical motion damping," in *Control Applications, 2002. Proceedings of the 2002 International Conference on*, 2002, pp. 304-309.
[13] S. Esteban, B. Andres-Toro, E. Besada-Portas, J. Giron-Sierra, and J. De la Cruz, "Multiobjective control of flaps and T-foil in high speed ships," in *Proceedings IFAC 2002 World Congress*, 2002.
[14] J. Giron-Sierra, S. Esteban, J. De la Cruz, B. De Andres, and J. Riola, "Fast ship's longitudinal motion attenuation with T-foil and flaps," in *Novel Vehicle Concepts and Emerging Vehicle Technologies Symposium*, 2003.
[15] S. Esteban, J. M. Giron-Sierra, B. de Andres-Toro, and J. M. De La Cruz, "Development of a control-oriented model of the vertical motions of a fast ferry," *Journal of ship research*, vol. 48, pp. 218-230, 2004.
[16] W.-Q. Lin and Z.-S. Dong, "Reducing the vertical motion in waves of round-bilge boat with controllable transom flaps," *International shipbuilding progress*, vol. 49, pp. 37-51, 2002.
[17] P. D. Sclavounos and H. Borgen, "Seakeeping analysis of a high-speed monohull with a motion-control bow hydrofoil," *Journal of ship research*, vol. 48, pp. 77-117, 2004.
[18] M. J. Hughes and K. M. Weems, "Time-domain seakeeping simulations for a high speed catamaran with an active ride control system," in *Proceedings of the 11th International Conference on Fast Sea Transportation, Hawaii, USA*, 2011.
[19] A. Rijkens, J. Keuning, and R. Huijsmans, "A computational tool for the design of ride control systems for fast planing vessels," *International shipbuilding progress*, vol. 58, pp. 165-190, 2011.
[20] A. Rijkens, H. Cleijsen, and J. Keuning, "On the hydrodynamic performance of an improved motion control device for fast ships," in *12th International Conference on Fast Sea Transportation*, 2013.
[21] J. Lavroff and M. R. Davis, "Slamming kinematics, impulse and energy transfer for wave-piercing catamarans," *Journal of Ship Research*, vol. 59, pp. 145-161, Sep 2015.
[22] J. Lavroff, M. R. Davis, D. S. Holloway, and G. Thomas, "The vibratory response of high-speed catamarans to slamming investigated by hydroelastic segmented model experiments," *International Journal of Maritime Engineering*, vol. 151, pp. 1-11, Oct-Dec 2009.
[23] J. Lavroff, M. R. Davis, D. S. Holloway, and G. Thomas, "Determination of wave slamming loads on high-speed catamarans by hydroelastic segmented model experiments," *International Journal of Maritime Engineering*, vol. 153, pp. A185-A197, Jul-Sep 2011.
[24] J. Lavroff, M. R. Davis, D. S. Holloway, and G. Thomas, "Wave slamming loads on wave-piercer catamarans operating at high-speed determined by hydro-elastic segmented model experiments," *Marine Structures*, vol. 33, pp. 120-142, Oct 2013.
[25] J. AlaviMehr, M. R. Davis, and J. Lavroff, "Low Reynolds Number Performance of a Model Scale T-Foil," *Royal Institution of Naval Architects. Transactions. Part A3. International Journal of Maritime Engineering*, vol. 157, pp. A175-A187, 2015.
[26] J. AlaviMehr, M. R. Davis, J. Lavroff, D. Holloway, and G. Thomas, "Response of a high-speed wave-piercing catamaran to an active ride control system," *Royal Institution of Naval Architects. Transactions. Part ~~A3~~A4. International Journal of Maritime Engineering, ~~In Press,~~*vol.158, pp. A325-A336, 2016.
[27] J. Bell, T. Arnold, J. Lavroff, and M. Davis, "Measured loading response of model motion control stern tabs," *Royal Institution of Naval Architects. Transactions. Part A. International Journal of Maritime Engineering*, vol. 155, pp. A1-A7, 2013.
[28] T. Shore, "Frequency response of motion controls on Incat catamaran model", BE Honours Thesis, University of Tasmania, 2011.
[29] F. Yang, "Experimental investigation on wave propagation in Australian Maritime College (AMC) towing tank and the performance of resistance and acoustic wave probes in static and moving condition," BE Honours Thesis, NCMEH, University of Tasmania, Australian Maritime College, 2015.
[30] J. F. O'Hanlon and M. E. McCauley, "Motion sickness incidence as a function of the frequency and acceleration of vertical sinusoidal motion," Human Factors Inc Report AD-76-215 for Unites States Office of Naval Research, September 1973.

9. Figures

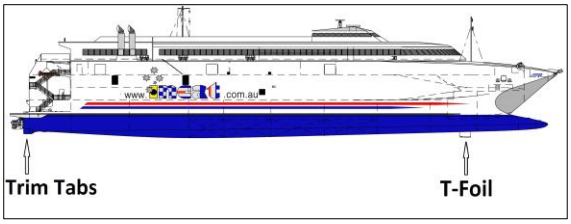

Figure 1: Location of the T-Foil and the trim tabs on a 112 m INCAT Tasmania high-speed wave-piercing catamaran [2].

Figure 2: Full scale T-Foil prior to installation on a 112 m INCAT Tasmania high-speed wave-piercing catamaran [2].

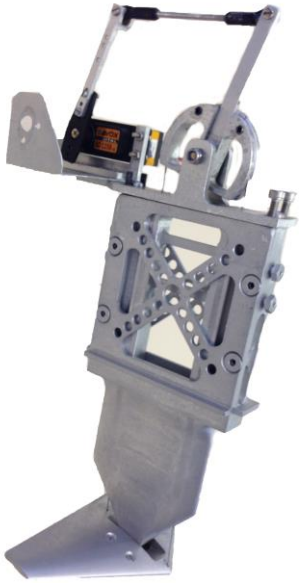

Figure 3: Electrically activated model scale T-Foil.

Figure 4: Electrically activated model scale stern tabs.

Figure 5: T-Foil installed on the aft section of the centre bow in a similar configuration to the full-scale INCAT 112 m vessel.

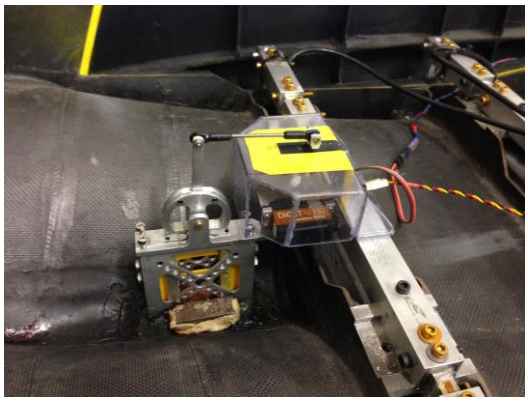

Figure 6: T-Foil electrical actuator installed in the centre bow of the model.

Figure 7: Stern tabs installed at the aft end of the model.

Figure 8: The catamaran model attached to the moving carriage.

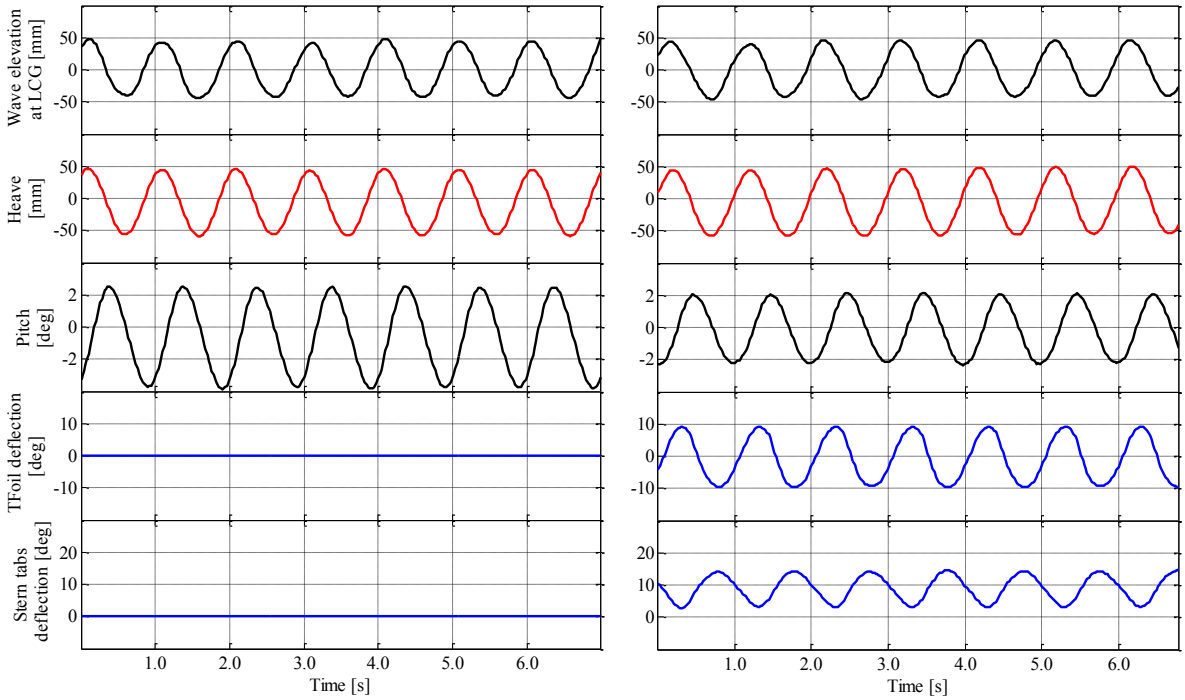

(a) Passive RCS mode (b) Pitch control mode

Figure 9: Time records at a model test speed of 2.89 m/s (Fr = 0.608), wave height of 90 mm and dimensionless wave encounter frequency $\omega_e^* = 3.182$: (a) Passive RCS mode, (b) Pitch control mode.

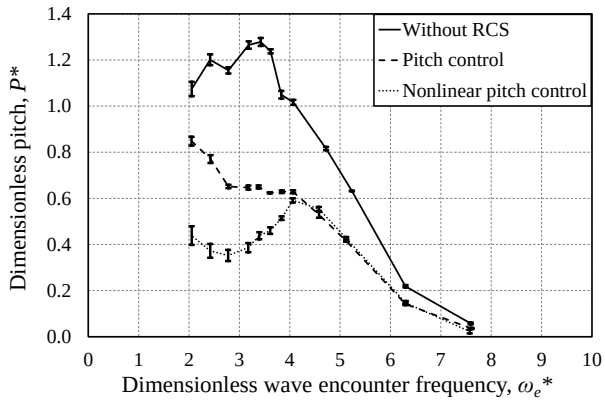

Figure 10: Pitch RAO at a model speed of 2.89 m/s (Fr = 0.608) and a wave height of 60 mm showing error bars.

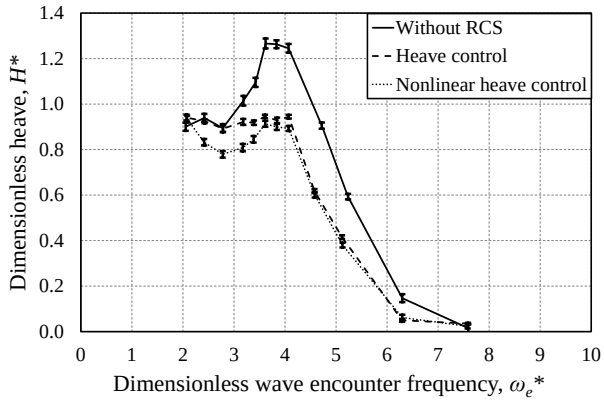

Figure 11: Heave RAO at a model speed of 2.89 m/s (Fr = 0.608) and a wave height of 60 mm showing error bars.

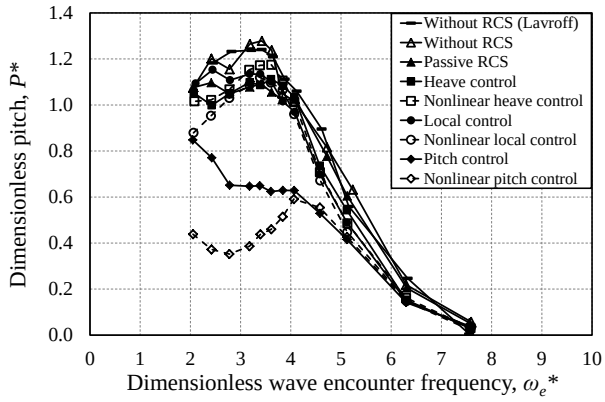

Figure 12: Pitch RAO at a model speed of 2.89 m/s (Fr = 0.608) and a wave height of 60 mm.

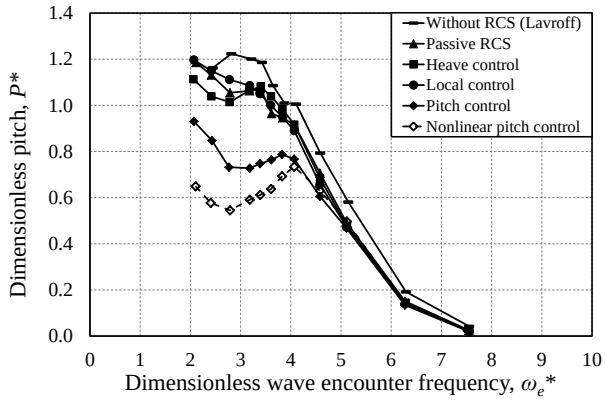

Figure 13: Pitch RAO at a model speed of 2.89 m/s (Fr = 0.608) and a wave height of 90 mm.

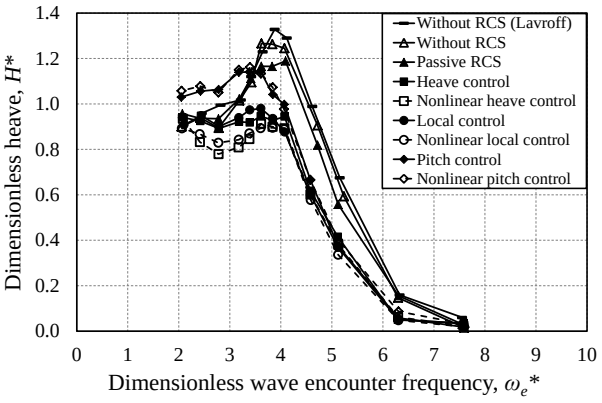

Figure 14: Heave RAO at a model speed of 2.89 m/s (Fr = 0.608) and a wave height of 60 mm.

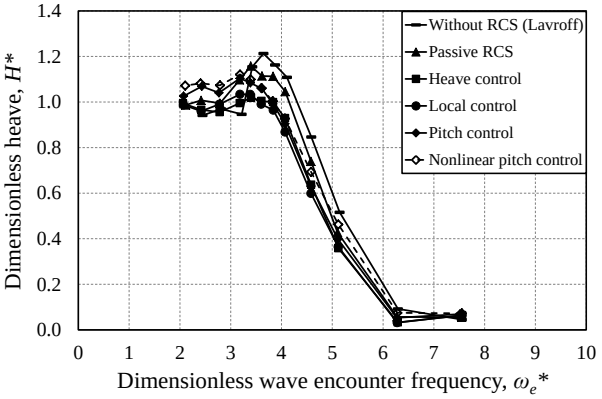

Figure 15: Heave RAO at a model speed of 2.89 m/s (Fr = 0.608) and a wave height of 90 mm.

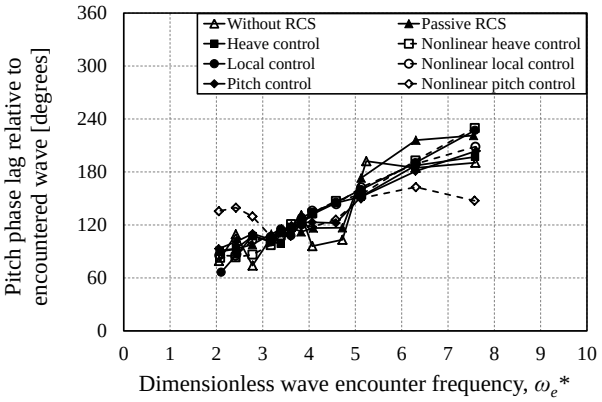

Figure 16: Pitch RPO (pitch phase lag relative to encountered wave at the LCG) at a model speed of 2.89 m/s (Fr = 0.608) and a wave height of 60 mm.

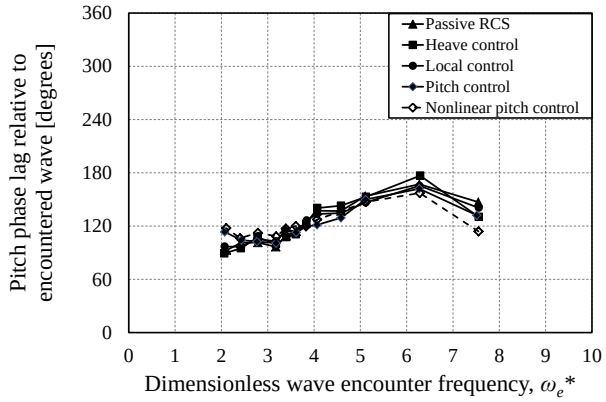

Figure 17: Pitch RPO (pitch phase lag relative to encountered wave at the LCG) at a model speed of 2.89 m/s (Fr = 0.608) and a wave height of 90 mm.

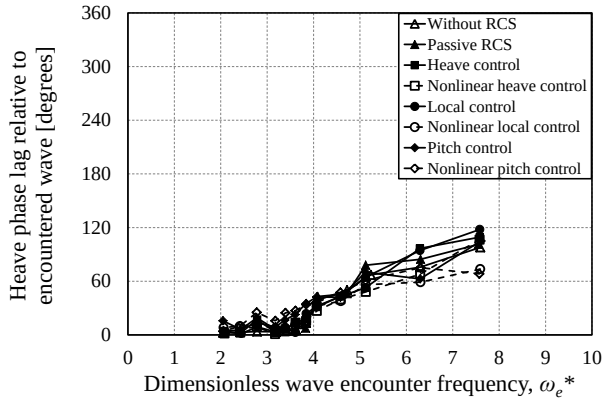

Figure 18: Heave RPO (heave phase lag relative to encountered wave at the LCG) at a model speed of 2.89 m/s (Fr = 0.608) and a wave height of 60 mm.

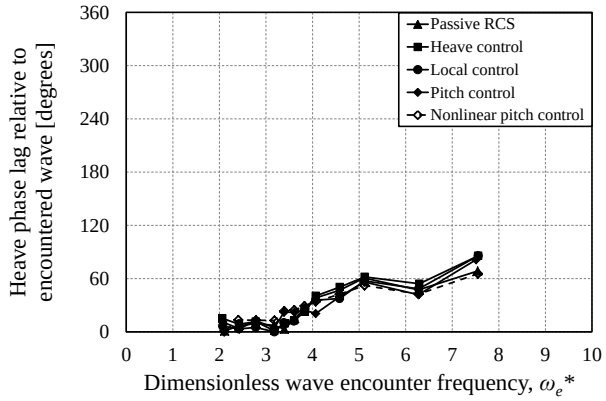

Figure 19: Heave RPO (heave phase lag relative to encountered wave at the LCG) at a model speed of 2.89 m/s (Fr = 0.608) and a wave height of 90 mm.

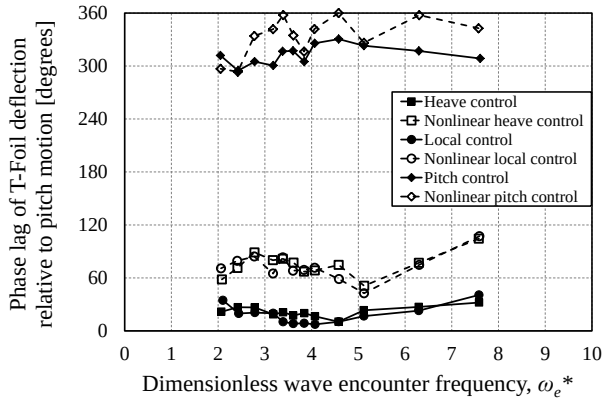

Figure 20: Phase lag of T-Foil deflection relative to pitch motion at a model speed of 2.89 m/s (Fr = 0.608) and a wave height of 60 mm.

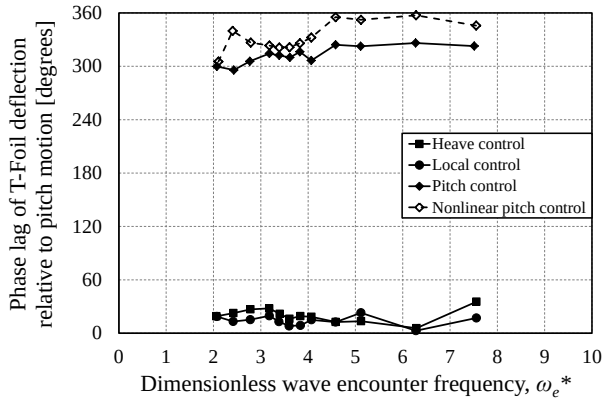

Figure 21: Phase lag of T-Foil deflection relative to pitch motion at a model speed of 2.89 m/s (Fr = 0.608) and a wave height of 90 mm.

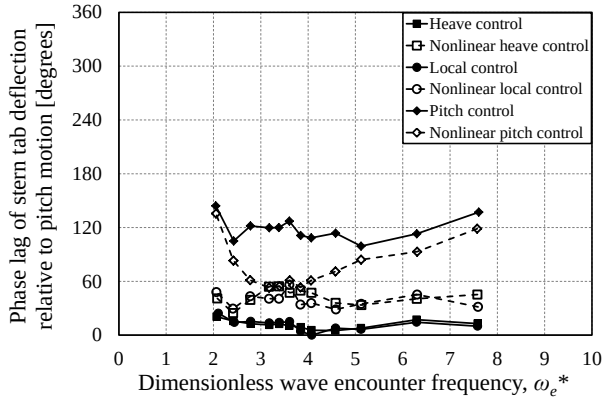

Figure 22: Phase lag of stern tabs deflection relative to pitch motion at a model speed of 2.89 m/s (Fr = 0.608) and a wave height of 60 mm.

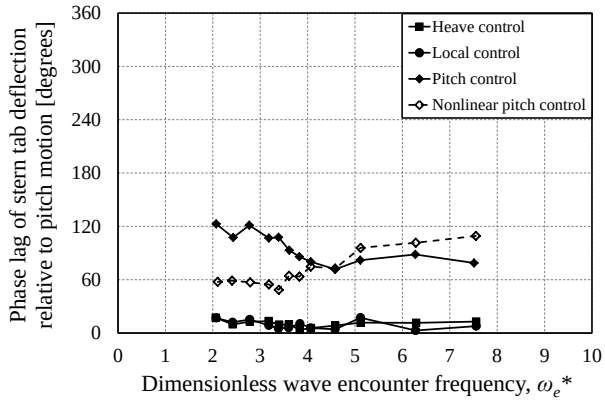

Figure 23: Phase lag of stern tabs deflection relative to pitch motion at a model speed of 2.89 m/s (Fr = 0.608) and a wave height of 90 mm.

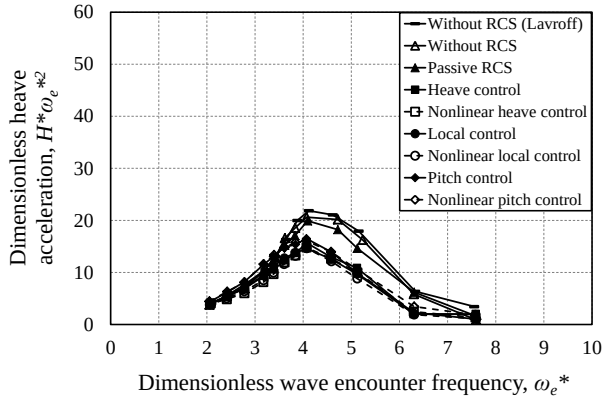

Figure 24: Dimensionless heave acceleration at LCG (37% LOA from the stern) at a model speed of 2.89 m/s (Fr = 0.608) and a wave height of 60 mm.

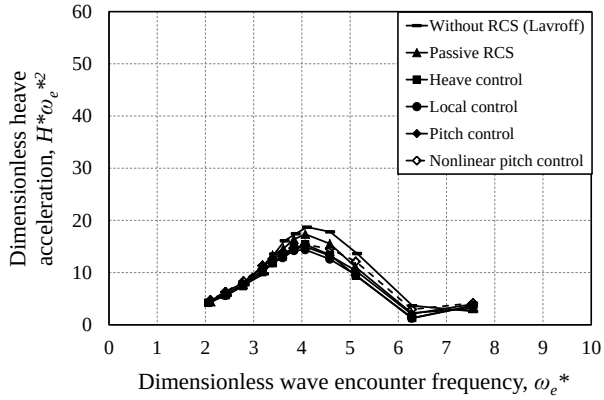

Figure 25: Dimensionless heave acceleration at LCG (37% LOA from the stern) at a model speed of 2.89 m/s (Fr = 0.608) and a wave height of 90 mm.

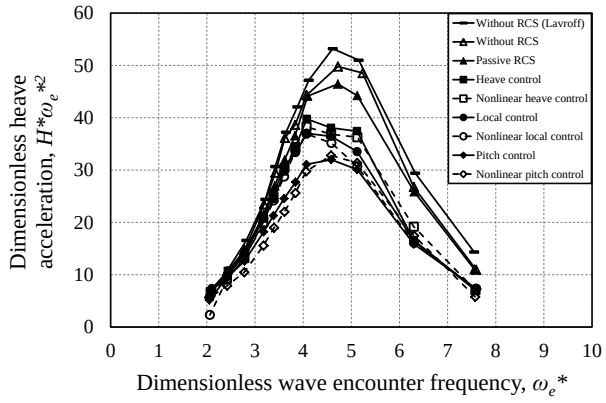

Figure 26: Dimensionless heave acceleration at the longitudinal location of the T-Foil (80% LOA from the stern) at a model speed of 2.89 m/s (Fr = 0.608) and a wave height of 60 mm.

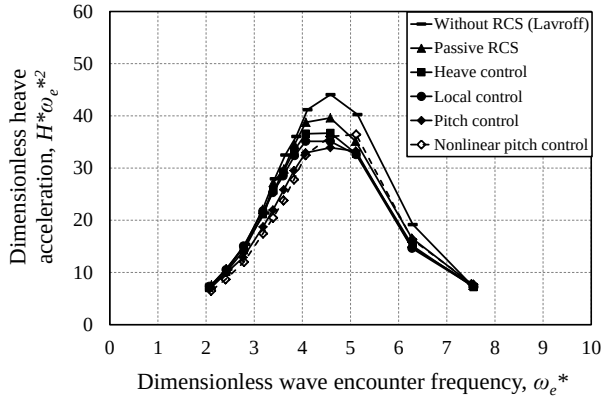

Figure 27: Dimensionless heave acceleration at the longitudinal location of the T-Foil (80% LOA from the stern) at a model speed of 2.89 m/s (Fr = 0.608) and a wave height of 90 mm.

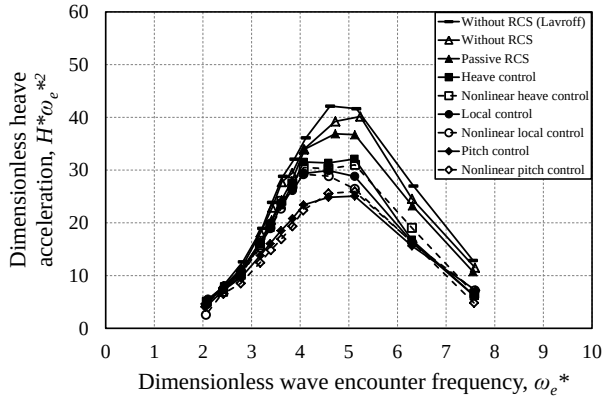

Figure 28: Dimensionless heave acceleration at the longitudinal location of the stern tabs at a model speed of 2.89 m/s (Fr = 0.608) and a wave height of 60 mm.

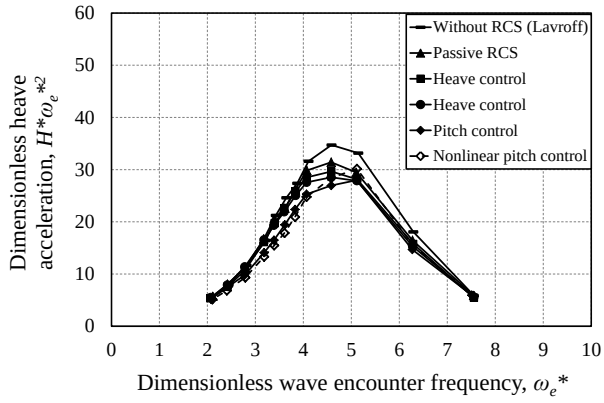

Figure 29: Dimensionless heave acceleration at the longitudinal location of the stern tabs at a model speed of 2.89 m/s (Fr = 0.608) and a wave height of 90 mm.

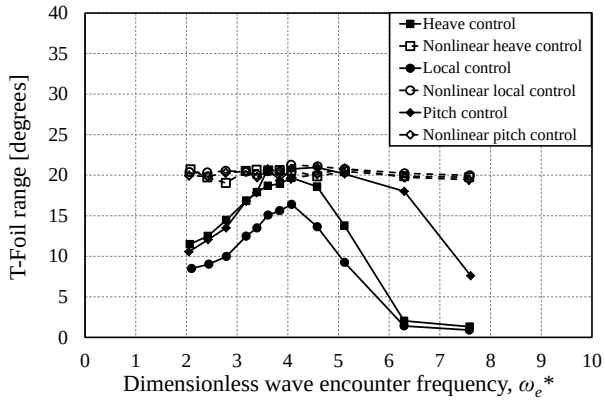

Figure 30: T-Foil deflection range at a model speed of 2.89 m/s (Fr = 0.608) and a wave height of 60 mm.

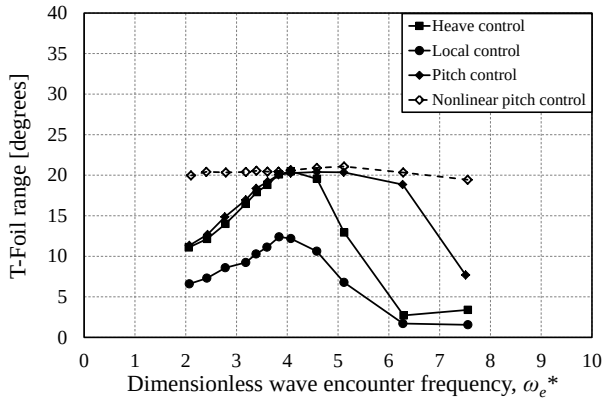

Figure 31: T-Foil deflection range at a model speed of 2.89 m/s (Fr = 0.608) and a wave height of 90 mm.

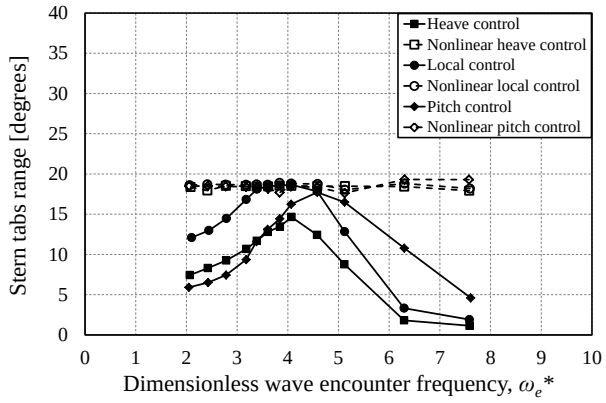

Figure 32: Stern tabs deflection range at a model speed of 2.89 m/s (Fr = 0.608) and a wave height of 60 mm.

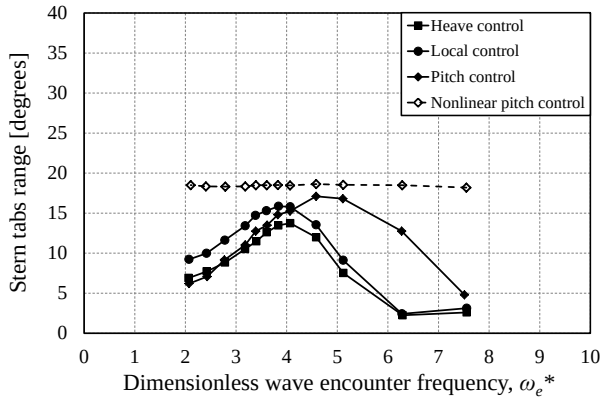

Figure 33: Stern tabs deflection range at a model speed of 2.89 m/s (Fr = 0.608) and a wave height of 90 mm.

10. Tables

Table 1: Specifications of the full scale 112 m INCAT catamaran and 2.5 m scaled model ride control surfaces.

		112 m full-scale (m)	2.5 m model scale (mm)
T-Foil	Chord	2.63	58.68
	Span	6.30	140.63
Stern tab	Chord	1.50	33.48
	Span	5.80	129.46

Table 2: Towing tank catamaran model RCS test conditions.

Model speed *U* (m/s)	Wave Height (mm)	Ride Control algorithm	Wave Frequency (Hz)
2.89	60	Without RCS	0.350 0.400 0.450 0.500 0.525 0.550 0.575 0.600 0.650 0.700 0.800 0.900
		Passive RCS	
		Heave control	
		Nonlinear heave control	
		Local control	
		Nonlinear local control	
		Pitch control	
		Nonlinear pitch control	
	90	Passive RCS	
		Heave control	
		Local control	
		Pitch control	
		Nonlinear pitch control	